

This discussion paper is/has been under review for the journal Biogeosciences (BG).
Please refer to the corresponding final paper in BG if available.

Seasonal methane accumulation and release from a gas emission site in the central North Sea

S. Mau¹, T. Gentz², J. H. Körber¹, M. Torres³, M. Römer¹, H. Sahling¹,
P. Wintersteller¹, R. Martinez², M. Schlüter², and E. Helmke²

¹MARUM – Center for Marine Environmental Sciences and Department of Geosciences,
University of Bremen, Klagenfurter Str., 28359 Bremen, Germany

²Alfred-Wegener-Institute for Polar and Marine Research, Am Handelshafen 12,
27570 Bremerhaven, Germany

³College of Earth, Ocean, and Atmospheric Sciences, Oregon State University, 104 CEOAS
Administration Building, Corvallis, OR 97331-5503, USA

Received: 10 October 2014 – Accepted: 20 November 2014 – Published: 19 December 2014

Correspondence to: S. Mau (smau@marum.de)

Published by Copernicus Publications on behalf of the European Geosciences Union.

Seasonal methane
accumulation and
release from a gas
emission site

S. Mau et al.

Title Page

Abstract

Introduction

Conclusions

References

Tables

Figures



Back

Close

Full Screen / Esc

Printer-friendly Version

Interactive Discussion



Abstract

Hydroacoustic data document the occurrence of 5 flare clusters and several single flares from which bubbles rise through the entire water column from an active seep site at 40 m water depth in the central North Sea. We investigated the difference in dissolved methane distributions along a 6 km transect crossing this seep site during a period of seasonal summer stratification (July 2013) and a period of well mixed winter water column (January 2014). Dissolved methane accumulated below the seasonal thermocline in summer with a median concentration of 390 nM, whereas during winter, methane concentrations were much lower (median concentration of 22 nM) and punctually elevated due to bubble transport. High resolution methane analysis by an underwater mass-spectrometer confirmed our summer results and were used to document prevailing stratification over the tidal cycle. Although sufficient methane was available, microbial methane oxidation was limited during both seasons. Measured and averaged rate constants (k') using Michaelis Menten kinetics were on the order of 0.01 days^{-1} , equivalent to a turnover time of 100 days. Time series measurements indicated an uptake of only 5–6% of the gas after 4 days, and no known methanotrophs and *pmoA*-genes were detected. Estimated methane fluxes indicate that horizontal eddy transport rapidly disperses dissolved methane, vertical transport becomes dominant during phases of high wind speeds, and relative to these processes, microbial methane oxidation appears to be comparably low. To bridge the discrete field data we developed a 1-D seasonal model using available year-long records of wind speed, surface temperature and thermocline depth. The model simulations show a peak release of methane at the beginning of fall when the water column becomes mixed. Consistent with our field data, inclusion of microbial methane oxidation does not change the model results significantly, thus microbial oxidation appears to be not sufficient to notably reduce methane during summer stratification before the peak release in fall.

Seasonal methane accumulation and release from a gas emission site

S. Mau et al.

Title Page

Abstract

Introduction

Conclusions

References

Tables

Figures



Back

Close

Full Screen / Esc

Printer-friendly Version

Interactive Discussion



1 Introduction

Methane is, after water vapor and CO₂, the most important greenhouse gas. Its concentration has increased by a factor of 2.5 since preindustrial times, from 722 ppb in 1750 to 1800 ppb in 2011 (IPCC, 2013). The total global emission was estimated to be ~ 550 Tg (methane) yr⁻¹ with an anthropogenic contribution of 50–65%. Geological sources, which were not considered in IPCC reports previously, are suggested to account for up to 30% of total emissions and include anthropogenic emissions related to leaks in the fossil fuel industry as well as natural geological seeps both terrestrial and marine (IPCC, 2013). In general, oceans have been found to be a minor source of methane to the atmosphere, accounting for 2–10% of the global emissions (Bange et al., 1994). An improved emission estimate from marine seeps suggests that these sources contribute ~ 20 Tg methane yr⁻¹, i.e., 4% of the global emissions, to the atmospheric methane (Etiope et al., 2008). A major fraction of the oceanic source (75%) is thought to originate from estuaries, shelf and coastal areas (Bange, 2006; Bange et al., 1994). For example, the European coastal areas were found to emit 0.46–1 Tgyr⁻¹, and thus contribute significantly to the overall global methane oceanic emissions (Bange, 2006). The author, however, points out that this estimate underestimates the coastal input, since fluxes from estuaries and shallow seeps are not adequately represented. Moreover, there is growing evidence that methane release from natural seepages and abandoned boreholes can significantly contribute to the global atmospheric methane emissions, especially from the North Sea (Judd et al., 1997; Rehder et al., 1998; Schroot et al., 2005).

It is important to consider shelf and coastal areas, as they are regions where most organic matter is deposited. Although continental margins account for only 10% of total ocean area and 20% of total ocean primary production (Killops and Killops, 1993), more than 90% of all organic carbon burial occurs in sediments depositing on deltas, continental shelves, and upper continental slopes (Bernier, 1989). At these

BGD

11, 18003–18044, 2014

Seasonal methane accumulation and release from a gas emission site

S. Mau et al.

Title Page

Abstract

Introduction

Conclusions

References

Tables

Figures



Back

Close

Full Screen / Esc

Printer-friendly Version

Interactive Discussion



Seasonal methane accumulation and release from a gas emission site

S. Mau et al.

Title Page

Abstract

Introduction

Conclusions

References

Tables

Figures

◀

▶

◀

▶

Back

Close

Full Screen / Esc

Printer-friendly Version

Interactive Discussion

5 locations, also characterized by high sedimentation rates, organic carbon is rapidly buried beneath the sulfate reduction zone, and becomes available to methanogens (e.g. Cicerone and Oremland, 1988). Methane is also generated by thermal breakdown at high temperature and pressure. A significant fraction of the formed methane is oxidized in anaerobic and aerobic sediments (e.g. Boetius et al., 2000; King, 1992), the remaining methane may be transported into the overlying water either dissolved in upwardly advecting pore waters or in case of oversaturation, in the form of gas bubbles. Because methane is undersaturated in seawater, rising methane bubbles partially dissolve during ascend through the water column (McGinnis et al., 2006), where the dissolved methane may be further consumed by microbial oxidation. Only if this methane survives transport to the mixed layer, can it be transferred to the atmosphere.

10 Using a bubble dissolution model in combination with acoustic observations of rising bubbles, McGinnis et al. (2006) showed that only bubbles emitted at shallow seeps (< 100 m) may reach the atmosphere. Methane rich bubbles from deeper seeps fully dissolve in the ocean. Model simulations based on methane concentrations, oxidation rates, and current records of two plumes observed in the Santa Barbara Basin indicate that half of the dissolved methane reaches the atmosphere and the other half is microbially oxidized of the shallow plume whereas the deeper plume is mostly oxidized (Mau et al., 2012). Thus, depending on the emission depth, methane remains in the ocean and can be microbially oxidized.

15 Shallow seeps thus are likely more important contributors to atmospheric methane. However, even at shallow seeps, density stratification may limit the vertical transport. For example, at the 70m deep Tommeliten area in the North Sea, less than ~ 4 % of the gas initially released at the seafloor reaches the mixed layer during summer, because a seasonal thermocline constrains methane transport to the atmosphere (Schneider von Deimling et al., 2011). Summer stratification traps methane beneath the thermocline, some of which may be consumed by microbial oxidation, and some will be released in the fall during first storm events. In order to investigate the seasonal

cycle of methane in the North Sea, we studied a shallow seep area both during summer (July 2013) when the water column was stratified, and in winter (January 2014) when the water column was well mixed.

1.1 Study site

5 The study site is situated in an area of active gas venting above a shallow gas reservoir in the central North Sea. The gas vents are located in the Netherlands sector, license block B13, south of Dogger Bank (Fig. 1). They occur at shallow water depth (< 45 m) in a flat region that lacks any morphological expression typical of seep structures (Schroot et al., 2005). These seeps are likely sourced from a biogenic methane reservoir ($\delta^{13}\text{C}$ values of -80‰ VPDB) of Pliocene to Pleistocene age, which lies 600–
10 700 m below the seafloor. Patches of gas saturated sediments from the gas reservoir to the seafloor have been imaged in seismic data. These data plus observations of separate vents in the water column and rapidly decreasing methane concentrations in cores with distance from the vent site led Schroot et al. (2005) to describe our study
15 site as a leaking gas reservoir with laterally discontinuous seepage.

Seasonal temperature stratification is a common feature in this and other shelf-seas, and it separates high-light and low-nutrient surface water from low-light and high-nutrient bottom water. Even though in some shelf areas, the tidal energy is sufficient to overcome stratification, models by Pingree and Griffiths (1978) and Holt and Umlauf
20 (2008) indicate that our study area is situated in a stratified region, east of the tidal front that surrounds the shallowest part of the Dogger bank. Thus, during spring and summer, the water column over the seeps investigated here, remains stratified over the course of a tidal cycle.

Seasonal methane accumulation and release from a gas emission site

S. Mau et al.

Title Page

Abstract

Introduction

Conclusions

References

Tables

Figures



Back

Close

Full Screen / Esc

Printer-friendly Version

Interactive Discussion



2 Methods

All data used in this study was collected during two cruises with R.V. *Heincke*. The first cruise (HE406) was conducted during summer 2013 (20–24 July), the second cruise (HE413) during winter 2014 (13–22 January).

2.1 EM710 flare imaging

During the winter cruise, we used a Kongsberg EM710 multibeam echosounder to map active gas emissions in the study area (Fig. 2). For the precise localization of individual flares, i.e., bubble streams in an echogram, the water column data were post-processed using the Fledermaus tools FMMidwater, DMagic, and the 3-D Editor (©QPS). The origin of individual flares was identified as the point of highest amplitudes near the seafloor. The coordinates of these points were extracted using the FMGeopicker and subsequently plotted on top of the bathymetry using ArcGIS 10.2 (ESRI).

For visualization of flare deflections and bubble rising heights, selected flares were extracted from the water column data as point data and edited using the 3-DEditor of DMagic (©QPS). The processed flares were plotted over the bathymetry data in a 3-D-view.

2.2 Water column sampling

To identify the size and magnitude of the dissolved methane plume generated by the bubble discharge, seawater was sampled along a transect crossing the active gas emission sites (Fig. 2). The transect, which extends 3 km to the east and 3 km to the west from a bubbling location (cluster 1 in Fig. 2) was sampled twice, once in summer 2013 and once in winter 2014. In both cases, the eastern sector (5 stations) was sampled on one day (~ 3 h) and the western sector (5 stations) on another day (~ 3 h), so that the center stations was sampled twice.

BGD

11, 18003–18044, 2014

Seasonal methane accumulation and release from a gas emission site

S. Mau et al.

Title Page

Abstract

Introduction

Conclusions

References

Tables

Figures

◀

▶

◀

▶

Back

Close

Full Screen / Esc

Printer-friendly Version

Interactive Discussion



Seasonal methane accumulation and release from a gas emission site

S. Mau et al.

Title Page

Abstract

Introduction

Conclusions

References

Tables

Figures



Back

Close

Full Screen / Esc

Printer-friendly Version

Interactive Discussion



Water samples were collected with a CTD/bottle rosette for methane concentration, methane oxidation rate, and molecular analyses. The rosette was equipped with twelve 5 L Niskin bottles, a Sea-Bird SBE 911 plus CTD, and an SBE 43 oxygen sensor for online monitoring of salinity, temperature, pressure, and dissolved oxygen. The data are archived in PANGAEA (doi:10.1594/PANGAEA.824863 and doi:10.1594/PANGAEA.832334). Twelve different water depths were sampled at each station for methane concentration analysis and 5 water depths for methane oxidation rates. Additional casts were needed to sample sufficient water for molecular analyses.

2.2.1 Methane concentration

For methane concentration analysis, samples were collected in 60 mL crimp-top glass bottles. All sample bottles were flushed with 2 volumes of water and filled completely to eliminate bubbles. Bottles were immediately capped with butyl rubber stoppers and crimp sealed. After adding 0.2 mL of 10 M NaOH to stop any microbial activity, a 5 mL headspace of pure N₂ was introduced into each bottle as described in Valentine et al. (2001) and the samples were stored at 4 °C. One to two aliquots of the headspace were analyzed to determine methane concentrations using a gaschromatograph equipped with a flame ionization detector. Analyses were performed both on board and post cruise. Replicate analyses of samples yielded a precision of ±5 %.

2.2.2 Methane oxidation rates

Methane oxidation (MO_x) rates were determined from ex situ incubations of water samples in 100 mL serum vials. Sampling and incubations were performed as described in Mau et al. (2013). Briefly, duplicate samples were collected: the set of samples taken at all stations was treated with 50 μL of ³H-labeled methane (160–210 kBq) in N₂, and a second sample set, which was collected at 5 stations in July 2013, was treated with 10 μL of ¹⁴C-labeled methane (12–15 kBq). After shaking the bottles to equilibrate the tracer with the water, the samples collected in summer 2013 were

Seasonal methane accumulation and release from a gas emission site

S. Mau et al.

Title Page

Abstract

Introduction

Conclusions

References

Tables

Figures

◀

▶

◀

▶

Back

Close

Full Screen / Esc

Printer-friendly Version

Interactive Discussion



incubated at 10 °C and those collected in winter 2014 at 9 °C. All samples were incubated in the dark for 24 h. After incubation, the total activity ($^3\text{H-CH}_4 + ^3\text{H-H}_2\text{O}$) in 1 mL aliquots was measured by wet scintillation counting, and the activity of $^3\text{H-H}_2\text{O}$ was measured after sparging the sample for > 30 min with N_2 to remove excess $^3\text{H-CH}_4$. Incubations with $^{14}\text{C-CH}_4$ were terminated by injecting 0.5 mL of 10 M NaOH. A 5 mL headspace was then added so that the remaining $^{14}\text{C-CH}_4$ accumulated in the headspace, while produced $^{14}\text{C-CO}_2$ and ^{14}C biomass was trapped in the aqueous NaOH solution. $^{14}\text{C-CH}_4$ in the headspace was combusted to $^{14}\text{C-CO}_2$, and $^{14}\text{C-CO}_3^{2-}$ was converted to $^{14}\text{C-CO}_2$ through acidification with HCl. The produced $^{14}\text{C-CO}_2$ was trapped in a solution of methoxyethanol and phenylethylamine, and the radioactivity was measured by wet scintillation counting.

MO_x rates were calculated assuming first-order kinetics (Reeburgh et al., 1991; Valentine et al., 2001):

$$\text{MO}_x = k' [\text{CH}_4] \quad (1)$$

where k' is the effective first-order rate constant calculated as the fraction of labeled methane oxidized per unit time, and $[\text{CH}_4]$ is the in situ methane concentration. To verify first order kinetics we conducted time series incubations and measured the tracer consumption after 1, 2, 3, and 4 days.

In addition, control samples were frequently taken and poisoned immediately after the addition of the tracer. The mean (\bar{x}) and SD (s) of all controls sampled during a cruise were calculated and the limit of detection (LOD) was set as:

$$\text{LOD} = \bar{x} + 3s \quad (2)$$

LOD was 0.02 nM day^{-1} for the summer 2013 survey, 0.09 nM day^{-1} for the winter 2014 survey, and $0.0005 \text{ nM day}^{-1}$ for the ^{14}C -methane survey in summer 2013.

The MO_x values were also corrected for differences between in situ and incubation temperatures (see the Supplement).

2.2.3 Analysis of bacterial communities

The composition of the bacterioplankton assemblages was examined using denaturing gradient gel electrophoresis (DGGE) based on the 16S rRNA gene as described in Mau et al. (2013). In short, immediately after sampling, bacterial cells were concentrated on Nuclepore filters (0.2 µm pore size). The filters were stored on board at -20 and at -80 °C post cruise. DNA was extracted by an UltraClean Soil DNA Kit (MoBio Laboratories, USA). 16S rRNA gene specific PCR was conducted using the forward primer GM5 plus GC-clamp and the reverse primer 907RM (Muyzer et al., 1993) under conditions described by Gerdes et al. (2005). The PCR products (ca. 500 bp) were analyzed by DGGE according to the protocol of Muyzer et al. (1993). Clearly visible bands of the DGGE gels were excised from the gel. The DNA was reamplified by PCR (Gerdes et al., 2005) and sequenced. The 16S rRNA gene sequences were taxonomically assigned by SILVA Online Aligner (Pruesse et al., 2012).

The presence of methane-oxidizing bacteria in the communities was checked by searching for genes encoding the particulate methane monooxygenase (pmoA), a key enzyme of methanotrophs (McDonald et al., 2008). The pmoA-gene-specific PCR reaction was conducted by using the primer set “pmoA” and amplification conditions described in McDonald and Murrell (1997).

2.3 Methane concentration analysis by underwater mass-spectrometry (UWMS)

In addition to the conventional methane analysis, in situ methane concentrations were detected and quantified with an UWMS (Inspectr200-200, Bell et al., 2007; Gentz et al., 2013; Schlüter and Gentz, 2008; Short et al., 2001; Wenner et al., 2004). The fast sampling frequency (≤ 2 s) of the UWMS allows mapping and quantification of methane in much higher resolution than the commonly used CTD/rosette-sampling technique. The instrument consists of a membrane inlet system (MIS), an Inficon (Bad Ragaz, Switzerland) Transpector CPM 200 quadruple mass spectrometer, a Varian (Palo Alto, USA) turbo pump, a roughing pump, a peristaltic pump (KC Denmark), and

BGD

11, 18003–18044, 2014

Seasonal methane accumulation and release from a gas emission site

S. Mau et al.

Title Page

Abstract

Introduction

Conclusions

References

Tables

Figures

⏪

⏩

◀

▶

Back

Close

Full Screen / Esc

Printer-friendly Version

Interactive Discussion



Seasonal methane accumulation and release from a gas emission site

S. Mau et al.

Title Page

Abstract

Introduction

Conclusions

References

Tables

Figures

◀

▶

◀

▶

Back

Close

Full Screen / Esc

Printer-friendly Version

Interactive Discussion



an embedded PC and a microcontroller. The UWMS was partly redesigned to include a cooling system (Ricor, K508), which lowers the detection limit for methane to 16 nM. The cooling system and the improvement of the detection limit are described in detail by Gentz and Schlüter (2012) and Schlüter and Gentz (2008). For reproducible gas permeation through the MIS, water is constantly heated to a steady temperature of 50°C and pumped at a flow rate of 3 mL min⁻¹ along the membrane by an external peristaltic pump.

The UWMS was deployed above the central gas seeps (cluster 1, Fig. 2) on 21 July 2013 (16:31–22:32 UTC) at five different water depths: just above the seafloor, 35, 28, 25, and 10 m. When the system had reached the respective depth, the research vessel moved slowly along a rectangular transect (~ 125 m S–N, ~ 150 m E–W, Fig. 2) surrounding the flares of cluster 1 (4°5.44′ N, 55°18.36′ E) and towed the UWMS, which continuously measured the methane concentrations. Each of the depth transects took about an hour and recorded 400–800 methane concentration values.

2.4 Estimation of methane fluxes

Horizontal and vertical turbulent diffusion, sea–air flux, and microbial oxidation were quantified for the upper (0–30 m) and lower water column (30–40 m) during summer stratification (July 2013) and for the entirely mixed water column (0–40 m) in winter (January 2014).

Turbulent horizontal and vertical diffusion (Diff) were calculated with Fick’s first law of diffusion as described in Mau et al. (2012):

$$\text{Diff} = D \left(\frac{\partial C}{\partial x} \right) \quad (3)$$

where D is the horizontal or vertical diffusion coefficient in $\text{m}^2 \text{s}^{-1}$. $\delta C / \delta x$ is the spatial concentration gradient in nM m^{-1} , estimated between the center and the outermost stations in the case of horizontal diffusion calculation, and the concentration gradient

between the lower and upper water column in the case of vertical diffusion, calculated only for summer 2013.

D_h , the horizontal diffusion coefficient, can range between 0.1 and 1000 m² s⁻¹ (Largier, 2003; Sundermeyer and Price, 1998) depending on the proximity to land. As the study area is located more than 230 km from shore, we used a D_h of 1000 m² s⁻¹ for our calculations. The vertical turbulent diffusion coefficient (D_v) can vary between 10⁻³ and 10⁻⁶ m² s⁻¹ depending on the energy in the water column (wind, tides, etc.) and stratification (Denman and Gargett, 1983; Wunsch and Ferrari, 2004). As a first approximation, we used 10⁻⁴ m² s⁻¹, which is a common cited value across the thermocline. The vertical eddy diffusion was estimated for all vertical profiles (all 10 CTD-stations).

The sea–air flux was calculated as described in Mau et al. (2007, 2012):

$$\text{SAF} = k_W(C_W - C_A) \quad (4)$$

where k_W is the gas transfer velocity in cm h⁻¹, C_W is the measured concentration of methane and C_A is the methane concentration in atmospheric equilibrium, both in nM. We calculated k_W , which depends on wind speed and the temperature-dependent Schmidt number of the gas, using parameterization developed by McGillis et al. (2001). Wind speed was recorded onboard and C_a was derived using the Bunsen solubilities given by Wiesenburg and Guinasso (1979) and measured ocean temperature and salinities. The sea air flux was calculated for surface water samples of all 10 stations sampled in summer 2013 and winter 2014.

The oxidative loss (OL) was calculated by depth integration of the MO_x rates:

$$\text{OL} = \bar{x}_{\text{MO}_x} z \quad (5)$$

where \bar{x}_{MO_x} is the averaged MO_x rate in nM day⁻¹ over the depth interval z in m. The depth interval is defined by the water stratification in the case of summer 2013 and covers the entire water depth in the case of winter 2014. Integration was done for all vertical profiles.

Seasonal methane accumulation and release from a gas emission site

S. Mau et al.

Title Page

Abstract

Introduction

Conclusions

References

Tables

Figures



Back

Close

Full Screen / Esc

Printer-friendly Version

Interactive Discussion



2.5 Seasonal model

A non-steady state, 1-D-model was developed to investigate the temporal evolution of methane over a year. We considered an entirely mixed water column during the winter month, stratification development during spring that lasted until early fall when the entire water column becomes mixed again. Hence, we considered one water layer during fall-winter (0–40 m) and two layers (upper and lower water column) during spring and summer. The initial model configuration was defined by the dissolved methane concentration observed in January 2014 (17 nM, excluding punctual high concentrations due to bubbles) and the transport and loss quantities calculated for the mixed water column condition in this month. We set the methane flux from the seafloor to be equal to the SAF estimate of January 2014. In daily time steps, the SAF and the vertical eddy diffusion were calculated using Eqs. (3) and (4) (above) and based on the amount of methane obtained in the previous time step. The parameters: mixed layer depth, wind speed, and surface water temperature were kept constant over a month, but then adjusted to the conditions of the following month. The mixed layer depth was determined from archived CTD-profiles (Pangaea) collected in an area extending from 3 to 6° E and from 54 to 56° N. Monthly mean wind speed was taken from the web-site: www.windfinder.com of the Ameland Oil Platform (mean of data from August 2010 to March 2014) and Forties/North Sea (mean of data from December 2012 to March 2014). Surface water temperatures were provided by the Bundesamt für Seeschifffahrt und Hydrographie (BSH).

3 Results

3.1 Seep locations

Echosounder data indicate bubble emission in the area of the sampled transect (Fig. 2). The center station was located at a known gas bubble emission site or flare cluster,

Seasonal methane accumulation and release from a gas emission site

S. Mau et al.

Title Page

Abstract

Introduction

Conclusions

References

Tables

Figures



Back

Close

Full Screen / Esc

Printer-friendly Version

Interactive Discussion



where several bubble streams occur in close proximity to each other. We observed an additional four flare clusters near the western sector of the transect, which displayed a similar seepage intensity as at the central seep site. In contrast, no additional flares were found in the area of the eastern sector. Although echosounder data point to bubbles rising to, or close to, the sea surface, no bubbles were visually identified at the sea surface due to rough sea state in winter 2014, however, surfacing gas bubbles were visually documented when the sea was calm in summer 2013. Seepage intensity showed no obvious variation related to tidal cycles, i.e., pressure variations due to high or low tides, rather, seeps were found to be active during all survey crossings.

3.2 Oceanographic setting

In summer (July 2013) a seasonal thermocline separated surface (0–30 m) from bottom water (30–42 m; Fig. 3). The surface water consisted of a 10 m thick mixed layer below which the temperature decreased stepwise from 17.5 to 7 °C in 30 m. Lower salinity was observed in 15 and 25 m depth, which departed from the general 34.55 PSU. The stepwise decrease in temperature and the salinity variations indicate the successive development of several pycnoclines driven by increasing sea surface temperatures and less wind activity in spring and summer. The oxygen concentrations increased from 220 μM at the surface to 240 μM at 30 m. In contrast to the surface water, the bottom water had a homogeneous temperature of 7 °C, a salinity of 34.63 PSU and contained less oxygen (190 μM).

In winter (January 2014) the entire water column was mixed (Fig. 3). The water had a temperature of 7 °C, a salinity of 34.85 PSU, a density of 27.3 kg m⁻³, and oxygen concentrations of 280 μM.

3.3 Methane concentrations

Consistent with the two layer structure observed by the temperature/salinity data, methane concentrations in summer 2013 also show a two layer distribution, with

higher concentrations in the bottom water relative to the surface values (Fig. 4a). Methane concentrations in the surface water range from 3.9 to 517.8 nM with a median of 32.5 nM. Methane concentrations in the bottom water range between 39.7 and 1627.7 nM with a median of 390.6 nM. Highest concentrations in the surface water were found near the center station (170 nM), which decreased to the outermost stations (to the west to 96 nM and to the east to 13 nM). However, the decrease is not continuous due to the presence of bubble emission sites in the area. Similarly, in the bottom water the highest methane concentrations were found at the center station (600–700 nM) decreasing unevenly towards the outmost stations (200–300 nM). In both layers the methane concentrations exceed the background concentration of 20 nM as measured at a reference station and reported in Grundwald et al. (2009). Even this background value is already oversaturated with respect to the atmospheric equilibrium concentration of 2.3–2.9 nM (at the relevant T/S conditions, Wiesenburg and Guinasso, 1979).

In winter 2014, much lower methane concentrations were found (Fig. 4b). Highest values were observed near the center site with concentrations of up to 656.6 nM. But such high concentrations decreased rapidly horizontally (within 1 km) and were not encountered during repeated measurements at the same location. The median of all methane concentration measurements along the transect is 22.4 nM, which is only slightly above the regional background concentration. In general, methane concentrations indicate a patchy distribution as expected in an active seep area.

3.4 UWMS methane concentrations

During the cruise in summer 2013, the UWMS was deployed in the vicinity of gas flare cluster 1 (Fig. 2). Because the instrument was towed close to several bubble streams, the recorded methane concentrations range over three orders of magnitude, from 0 to 2127 nM in surface water (transects in 10, 25, 28 m) and from 259 to 2213 nM in the bottom water (transects in 30 and 40 m) (Fig. 4c). Nonetheless, the general pattern of lower methane concentrations in the surface and higher concentrations in the bottom

Seasonal methane accumulation and release from a gas emission site

S. Mau et al.

Title Page

Abstract

Introduction

Conclusions

References

Tables

Figures

◀

▶

◀

▶

Back

Close

Full Screen / Esc

Printer-friendly Version

Interactive Discussion



water observed by conventional methods (see Sect. 3.3) is also apparent in the UWMS-data. The median values of the records in 10, 25, and 28 m water depth range from 54 to 402 nM and in 30 and 40 m depth, the medians range from 512 to 793 nM.

The UWMS measured the methane during **ebbing tides, where** water levels fell from 0.18 to -0.27 m, whereas CTD/rosette samples were collected during rising tides, when sea level height increased from -0.21 to 0.06 m and from 0.04 to 0.16 m (Figure S1 in the Supplement). Again, the general pattern of lower concentrations in the surface and higher ones in the bottom water was apparent in all stations, even though methane data were obtained during different tidal phases.

3.5 Methane oxidation

Similar to the distribution of methane and co-located oceanographic data, MO_x rates in summer 2013 show a two layer pattern whereas MO_x measured in winter 2014 are uniform throughout the water column (**Fig. 5a, b**). In summer, significantly less methane was oxidized in the surface water relative to the bottom water. In the surface waters MO_x -rates ranged between 0.04 and 92.64 $nMday^{-1}$ with a median of 0.10 $nMday^{-1}$ and in the bottom water between 1.60 and 840.93 $nMday^{-1}$ with a median of 3.99 $nMday^{-1}$. The total range of both layers (0.04–840.93 $nMday^{-1}$) exceeds the range of MO_x -rates observed during the winter survey (0.09–8.72 $nMday^{-1}$). The median of all MO_x -rates measured in January 2014 was 0.24 $nMday^{-1}$.

Time series and ^{14}C -methane tracer incubations indicate a slow oxidation rate of methane over time. Although the methane concentrations greatly differ during both seasons, only 5–6% of the 3H -methane tracer was utilized during 4 d of incubation (Fig. 5d). In the ^{14}C -methane tracer experiments, a significantly higher concentration of methane is added to the sample relative to the 3H -methane tracer additions (Mau et al., 2013). However, even the elevated methane additions did not lead to a higher methane utilization. The MO_x -rates determined using ^{14}C -methane tracer additions range from **0.0009 to 0.04 $nMday^{-1}$** with a median of **0.003 $nMday^{-1}$** in the surface

BGD

11, 18003–18044, 2014

Seasonal methane accumulation and release from a gas emission site

S. Mau et al.

Title Page

Abstract

Introduction

Conclusions

References

Tables

Figures

⏪

⏩

◀

▶

Back

Close

Full Screen / Esc

Printer-friendly Version

Interactive Discussion



water (Fig. 5c). In the bottom water, the values range from 0.05 to 0.53 nM day⁻¹, with a median of 0.16 nM day⁻¹. Even though the ¹⁴C-MO_x-rates were lower than the ones obtained with the ³H-methane tracer, in both cases the two layer structure was obvious for the summer 2013 situation.

3.6 Microbial communities

Molecular samples taken in summer 2013 show also a difference between surface and deep waters, whereas winter 2014 samples indicate a homogeneous distribution of microorganisms (Fig. 6, Table 1). In summer 2013, different DGGE banding patterns reveal the changes in microbial communities with depth. The surface water samples showed two strong bands (6, 7) that could be affiliated to the *Rhodobacteracea* and two bands that could be assigned to the *Cyanobacteria/Synechococcus* clade (8, 9). The middle and bottom water samples were characterized by a strong chloroplast band (2), but showed also bands affiliated to the *Rhodobacteracea* (5, 6). In the bottom water samples of the central station, we found an additional band, assigned to *Pseudoalteromonas* (10). The gel pattern of the winter samples showed no significant bands. The sequences of the faint bands excised were of low quality. Only two of the bands could be assigned to the *Rhodospirillaceae* (12, 13).

Neither the summer nor the winter bacterial communities exhibited known methanotrophic bacteria, even though the samples originate from an actively gas venting area. The absence of methanotrophic bacteria was further supported by the negative results of the pmoA-PCRs that targets a methanotroph molecular marker gene.

BGD

11, 18003–18044, 2014

Seasonal methane accumulation and release from a gas emission site

S. Mau et al.

Title Page

Abstract

Introduction

Conclusions

References

Tables

Figures



Back

Close

Full Screen / Esc

Printer-friendly Version

Interactive Discussion



4 Discussion

4.1 Distribution of methane in summer and winter

Our highest dissolved methane concentrations measured in the bottom water reach magnitudes similar to those observed at other shallow seep sites (Table 2). Our highest value of 1627.7 nM is comparable to measurements near the Coal Oil Point seep field, Santa Barbara Basin, California (up to 1900 nM, Mau et al., 2012), and it is higher than methane concentrations reported for the Tommeliten, North Sea (268 nM, Schneider von Deimling et al., 2011), and offshore Svalbard, west of Prins Karls Forland (524 nM, Gentz et al., 2013).

Even though gas bubbling was observed at the sea surface in summer months, the dissolved methane at these and also at other vent sites, is trapped beneath a thermocline or halocline, which hampers further ascend of the dissolved methane to the atmosphere. The studied seeps are located at a depth of 40 m and the dissolved methane plume was found beneath a seasonal thermocline. At the Tommeliten seep site, the methane plume was also observed beneath the seasonal thermocline (Schneider von Deimling et al., 2011) whereas the methane plume originating from the 245 m deep seeps offshore Prins Karls Forland was confined to water depths beneath a local halocline (Gentz et al., 2013). In the Baltic Sea, summer stratification also leads to accumulation of methane below the thermocline (Gülzow et al., 2013). At all these sites, an enhanced release of methane to the atmosphere is thought to occur upon erosion of stratification. In contrast, the dissolved methane plume originating from seeps situated between 5 and 70 m at the Coal Oil Point is dispersed above the thermocline within the mixed layer (Mau et al., 2012), and as such is not controlled by seasonal stratification patterns.

Trapping and accumulation of dissolved methane beneath a thermocline is also well documented in lakes, where thermal stratification separates methane-poor, surface water from the methane-rich, but anoxic, bottom water in e.g. a shallow floodplain lake in south-eastern Australia (Ford et al., 2002), in a polyhumic lake in southern

Seasonal methane accumulation and release from a gas emission site

S. Mau et al.

Title Page

Abstract

Introduction

Conclusions

References

Tables

Figures



Back

Close

Full Screen / Esc

Printer-friendly Version

Interactive Discussion



Finland (Kankaala et al., 2007), and in the subtropical Lake Kinneret in Israel (Eckert and Conrad, 2007). The accumulated methane is released when water starts mixing driven by enhanced wind forcing and lower temperatures.

Our results verify the assumption that in a stratified-controlled system, no methane accumulation occurs in **winter, when the water column is well mixed as** indicated by vertical profiles of temperature, salinity, and oxygen. During our winter field program, methane concentrations were found to deviate only due to bubble ascent and were otherwise low and constant throughout the water. The median winter concentration of 22 nM is similar to the background methane concentrations of 20 nM reported by Grunwald et al. (2009) for the German Bight, but the concentration is elevated relative to water originating from the Atlantic Ocean, which carry 2.5–3.5 nM of methane (Rehder et al., 1998) and to the methane background concentrations of < 5 nM at the Tommeliten (Niemann et al., 2005; Schneider von Deimling et al., 2011).

4.2 **Low methane oxidation**

Measured MO_x -rates at our study site lie at the upper end of MO_x -rates previously reported, which span over six orders of magnitude from 0.001 to 1000 nM day^{-1} (Table 2 and summarized in Fig. 1 in Mau et al., 2013). The rates measured in deep water samples during summer (median 3.9 nM day^{-1} , up to 840 nM day^{-1}) equal those observed in the Gulf of Mexico (median 10 nM day^{-1} , up to 820 nM day^{-1}) (Valentine et al., 2010). Even winter time rates are high in comparison to rates measured in the Eel River Basin, an area of hydrate dissociation (Valentine et al., 2001) and match rates of the Coal Oil Point seep field in the Santa Barbara Basin (Mau et al., 2012; Pack et al., 2011).

However, we note that in spite of the reported high MO_x values, detailed analysis of the data reveals an overall low activity of methane oxidizing microorganisms. This apparent contradiction arises from the fact that the MO_x -rate of a given sample is traditionally calculated by multiplying methane concentration with the fraction of the tracer converted per unit time, i.e., k' – the first order rate constant. At a given k' value

changes in methane concentrations yield MO_x -rates that are low or high depending on whether methane concentrations are low or high. Thus high MO_x -rates might just reflect high methane concentrations, and not necessarily a rapid turnover rate. The constant k' provides an indication of the relative activity in a water sample (Koschel, 1980), but it cannot be viewed independently from methane concentration, as k' is derived from tracer conversion in a sample with ambient methane concentration.

Alternatively, the MO_x -rate can be plotted against methane concentration, following the approach used by Michaelis Menten (MM) kinetics to describe the rate of a first order enzymatic reaction that depends on one substrate, by relating the reaction rate (V) to the substrate concentration (S) (Fig. 7). The model takes the form of the equation:

$$V = v_{\max} \frac{S}{(K_m + S)} \quad (6)$$

where v_{\max} is the maximum uptake rate and K_m is the concentration at which the reaction rate is half of v_{\max} . As illustrated in Fig. 7, the enzymatic uptake can be very rapid as soon as methane is available and levels off when enzyme saturation is reached (low K_m and high v_{\max} , MM-kinetics 1), however, in some systems the uptake can be very slow, and enzyme saturation reached at very high methane concentrations (high K_m and low v_{\max} , MM-kinetics 2). K_m values of cultured and uncultured soil methane oxidizing bacteria range between 0.8 and 12 μM (Baani and Liesack, 2008; Bender and Conrad, 1993). For v_{\max} , we used MO_x -rate maxima reported for oceanic environments, which range between 100 and 1000 nM day^{-1} (Mau et al., 2013). Using these wide data ranges, we depict the predictive behavior using both end-member for MM kinetics. Apart from 7 data points, which were collected in the bottom water close to flare cluster 1 (stations S12 and S13, Fig. 2), all other data points are close to a curve that follows MM-kinetics 2, with high K_m value and low v_{\max} , hence pointing to a generally slow uptake and oxidation of methane.

Using the MM curve on which most of our data plot, we can derive an overall k' value from the slope of the linear portion of the curve (Fig. 7), which for our case is 0.01 d^{-1} .

BGD

11, 18003–18044, 2014

Seasonal methane accumulation and release from a gas emission site

S. Mau et al.

Title Page

Abstract

Introduction

Conclusions

References

Tables

Figures



Back

Close

Full Screen / Esc

Printer-friendly Version

Interactive Discussion



Seasonal methane accumulation and release from a gas emission site

S. Mau et al.

Title Page

Abstract

Introduction

Conclusions

References

Tables

Figures

◀

▶

◀

▶

Back

Close

Full Screen / Esc

Printer-friendly Version

Interactive Discussion



As expected this value matches the majority of the measured k' values (median of summer data: 0.02 d^{-1} , median of winter data: 0.01 d^{-1}) as well as the value k' derived from the time series incubations (0.01 d^{-1} , $n = 4$). We pose that, rather than using MO_x -rates, or k' values from individual samples, MM kinetics fit to the data provides an effective way to generate an overall parameter k' from an entire data set, which best reflects the ecosystem microbial activity. The inverse of the modelled k' gives a turnover time of 100 d suggesting a rather low activity of methane-oxidizing bacteria in both summer and winter.

The low activity of methane oxidizing microorganisms obtained from the MM approach is further supported by time series experiments, ^{14}C -methane spike experiments, and molecular analysis of filtered matter from seawater. Time series incubations show a slow uptake of methane over time, solely 5–6% of the added ^3H -methane-tracer was converted after 4 days. Even when we spiked the sample with elevated ^{14}C -methane concentrations of 400–500 nM, there was no additional substrate utilized after incubation for one day, indicating that methane oxidizing microorganisms cannot rapidly consume the additional methane. Consistently, DGGE and *pmoA* analysis did not reveal the presence of any known methanotrophic bacteria or *pmoA*-genes. We note, however, active pelagic methanotrophic populations remain largely uncharacterized (Valentine, 2011) and that molecular studies continue to reveal novel sequences closely related to those coding for methane monooxygenase (Elsaied et al., 2004; Tavormina et al., 2008; Wasmund et al., 2009), an enzymatic hallmark of aerobic methanotrophs.

4.3 Transport is faster than methane oxidation

Most likely, a significant component of the methane flux to the atmosphere is supported by direct transport of methane gas as bubbles. That component is being constrained by video observations and gas bubble samples (T. Gentz, personal communication, 2014); here, we focus on the fate of the dissolved methane fraction. When methane enters the water column, it is transported by ocean currents and it spreads by horizontal

Seasonal methane accumulation and release from a gas emission site

S. Mau et al.

[Title Page](#)[Abstract](#)[Introduction](#)[Conclusions](#)[References](#)[Tables](#)[Figures](#)[◀](#)[▶](#)[◀](#)[▶](#)[Back](#)[Close](#)[Full Screen / Esc](#)[Printer-friendly Version](#)[Interactive Discussion](#)

and vertical eddy diffusion. Dissolved methane can then support methane oxidizing microorganisms and if water with methane concentrations higher than saturation reach the mixed layer, methane will be transferred into the atmosphere. In order to evaluate the relative importance of these transport and loss processes, we estimated the horizontal and vertical eddy diffusion, sea–air flux, and integrated the MO_x -rates over the water depth (see methods). **The advective transport by ocean currents was not estimated as this process does not decrease the concentration of methane, but solely transports methane from the seep site in direction of the current flow.** All fluxes were estimated in units of $\text{nmol m}^{-2} \text{s}^{-1}$. As shown in Fig. 8, we estimated summer fluxes for the bottom (30–43 m) and surface waters (0–30 m), using data collected in July 2013, and winter fluxes for the entire unstratified water column (0–42 m) using data from January 2014. The results show that the horizontal eddy diffusion is the dominant process that rapidly dilutes the emitted methane. The loss processes, i.e., sea air flux and microbial oxidation, are more than 4-orders of magnitude lower than the horizontal eddy diffusion. Our flux estimates revealed that in summer more methane is transported via vertical diffusion into the surface water than is oxidized in the bottom water. In the surface water, 50% is oxidized and the other 50% is transferred into the atmosphere. In winter, the sea air flux removes more methane from the water column due to increased wind speed. Overall the flux estimates indicate that diffusion (dilution of the methane rich water with background ocean water) outcompetes microbial methane oxidation.

All of these flux estimates may vary by up to one order of magnitude. The estimates were determined as described by Mau et al. (2012), which includes a detailed discussion of the uncertainties associated with the calculations. Briefly, the uncertainty originates from the precision of the different measurements, assumed diffusion coefficients, and the parameterization of the gas transfer velocity. The uncertainty does not include any possible variations during the 3 h of sampling. Although the estimates can vary considerably, horizontal diffusion of methane remains consistently higher than vertical diffusion and methane oxidation.

Our flux estimates, although subject to high uncertainties, suggest that microbial oxidation is of minor importance in the central North Sea. Particularly during periods of high wind speed (fall and winter), more methane reaches the atmosphere than is oxidized in the water. In summer when lower wind speeds prevail, methane oxidation is similar in magnitude to the gas transfer to the atmosphere. Our findings are similar to those reported by Scranton and McShane (1991), who conclude that methane oxidation constitutes a relatively small sink for methane in the Southern Bight of the North Sea ($0.00023\text{--}0.3\text{ nM day}^{-1}$), relative to methane losses to the atmosphere ($0.00026\text{--}7.5\text{ nM day}^{-1}$), which are highest during periods of high wind speed. The data are consistent with estimates done for the shallow Coal Oil Point methane plume in the Santa Barbara Basin (Mau et al., 2012). There, 0.05 mol d^{-1} are oxidized in the surface water and 0.03 mol d^{-1} are transferred to the atmosphere.

4.4 Modeled methane accumulation and flux to the atmosphere over a year

To extend our inferences based on 2 field programs to seasonal changes over an entire year, we developed a 1-D model using wind speed, sea surface temperature, and the depth of the mixed layer defined by the depth of the thermocline. CTD data of the surveyed region were used to specify the monthly development of the mixed layer depth, which develops in May and deepens until the entire water column becomes mixed in September (Fig. 9d). The model focused on the sinks of dissolved methane: sea air flux and microbial methane oxidation.

Three simulation were run. The first simulation included solely the vertical transport (sea air flux and vertical eddy diffusion during stratification), the second tested the uncertainty of the first simulation due to the most unspecified parameter, D_v , and the third simulation included the microbial methane oxidation (Fig. 9a–c).

Model results of the first simulation, which do not include methane oxidation, illustrate the seasonal changes in methane concentrations. With decreasing wind speed in spring, methane concentration slowly rise in the water column; at the onset of stratification, most of the dissolved methane accumulates in the bottom water,

BGD

11, 18003–18044, 2014

Seasonal methane accumulation and release from a gas emission site

S. Mau et al.

Title Page

Abstract

Introduction

Conclusions

References

Tables

Figures

⏪

⏩

◀

▶

Back

Close

Full Screen / Esc

Printer-friendly Version

Interactive Discussion



**Seasonal methane
accumulation and
release from a gas
emission site**

S. Mau et al.

[Title Page](#)[Abstract](#)[Introduction](#)[Conclusions](#)[References](#)[Tables](#)[Figures](#)[◀](#)[▶](#)[◀](#)[▶](#)[Back](#)[Close](#)[Full Screen / Esc](#)[Printer-friendly Version](#)[Interactive Discussion](#)

5 leaving the surface water as the only source of methane to the atmosphere and, thus, reducing the methane concentrations in the surface water. As the concentration gradient between bottom and surface increases, more methane is transferred to the surface water by vertical eddy diffusion; that added to lower wind speeds in the summer
10 cause methane concentrations to increase in the surface water. In late summer, beginning of fall, the mixed layer depth deepens due to increased wind forcing. Surface and bottom waters become mixed leading to a peak in methane concentration in the entire water column, which is transferred to the atmosphere by sea air exchange. Due to prevailing high wind speeds in fall and winter, methane concentrations rapidly
15 decrease to a background concentration level of 20 nM.

The first simulation is greatly dependent on the vertical diffusion coefficient D_v . This parameter could be one order higher ($10^{-3} \text{ m}^2 \text{ s}^{-1}$) due to shallow water depth or one order lower ($10^{-5} \text{ m}^2 \text{ s}^{-1}$) due to low wind speed especially in summer. For example, during the first sampling period in July 2013 a wind speed of $2\text{--}3 \text{ m s}^{-1}$ was recorded
20 whereas the average value used for the month July in the model was 7 m s^{-1} . Therefore, we tested the uncertainty of the model that results from the variability in D_v in the second simulation. The results of these simulations show that the modelled trend would be exaggerated if transport is less ($D_v = 10^{-5} \text{ m}^2 \text{ s}^{-1}$), that is, e.g. a larger methane peak is predicted at beginning of fall, which would be smoothed if we were to use
25 a higher D_v ($10^{-3} \text{ m}^2 \text{ s}^{-1}$). The best fit to the data is achieved using a D_v of $10^{-4} \text{ m}^2 \text{ s}^{-1}$, which yields a methane concentration of 39 nM in the surface water for the month July, similar to the median of the measurements, 33 nM. A methane concentration of 260 nM is predicted for the bottom water, which is equivalent in magnitude to the median of our measurements, 390 nM.

After obtaining of the best fitting D_v , we included methane oxidation in the third model simulation. For this, we subtracted the averaged measured MO_x rates from the surface and bottom water reservoirs. MO_x was included in the surface water all year round, but in the bottom layer (i.e., in case of stratification) MO_x was considered only when sufficient methane has accumulated, that is, for the month May we assume a negligible

MO_x in the bottom water. The model results do not show any significant difference by comparison to the first simulation (which included only transport) except for the month of June, when the model predicts significant methane consumption by MO_x in the bottom water. Due to this decrease of methane concentration in the bottom water, the concentration difference between the surface and bottom water is not as large anymore and, therefore, less methane is transferred by vertical eddy diffusion into the surface water. The simulation drives the concentration gradient to equilibrium, until the water column becomes fully mixed. We note that the model predicts a similar quantity of methane released to the atmosphere at the beginning of fall whether or not methane oxidation is included in the simulation.

In summary, if D_v is below $10^{-4} \text{ m}^2 \text{ s}^{-1}$, then a peak release of methane occurs at the beginning of fall when the water column becomes mixed. Microbial methane oxidation appears insufficient to significantly reduce methane before the peak release in fall.

The model is also used to estimate an annual methane emission of 0.027 mol m^{-2} . This estimate is 3–8 times higher than the general European shelf estimate of $0.0035\text{--}0.0076 \text{ mol methane m}^{-2} \text{ yr}^{-1}$ proposed by Bange (2006). The highly elevated flux above a seep area documented by our work, confirms the expectation of Bange (2006) that his general European shelf flux estimate might be an underestimation since shallow seeps were not sufficiently represented in his work. Moreover, our flux estimate still does not include the fraction of methane directly transported by bubbles to the sea surface, which increases the total methane transfer to the atmosphere even more.

5 Conclusions

1. Observations at a shallow gas seep site in the central North Sea document methane accumulation below the thermocline during summer stratification, but no methane accumulation in the winter. Similar summer time results are presented by Schneider von Deimling (2011) for the Tommeliten area in the northern North Sea.

BGD

11, 18003–18044, 2014

Seasonal methane accumulation and release from a gas emission site

S. Mau et al.

[Title Page](#)

[Abstract](#)

[Introduction](#)

[Conclusions](#)

[References](#)

[Tables](#)

[Figures](#)

[◀](#)

[▶](#)

[◀](#)

[▶](#)

[Back](#)

[Close](#)

[Full Screen / Esc](#)

[Printer-friendly Version](#)

[Interactive Discussion](#)



Seasonal methane accumulation and release from a gas emission site

 S. Mau et al.

[Title Page](#)
[Abstract](#)
[Introduction](#)
[Conclusions](#)
[References](#)
[Tables](#)
[Figures](#)

[Back](#)
[Close](#)
[Full Screen / Esc](#)
[Printer-friendly Version](#)
[Interactive Discussion](#)

2. Our seasonal model bridges our summer and winter field studies and predicts an enhanced sea–air flux at the end of the stratification period. Such an elevated sea–air methane transfer was measured in the Baltic Sea when wind forcing increased after the summer month breaking down the stratification (Gülzow et al., 2013). The seasonality in fluxes highlights the importance of understanding the effect of seasonal changes on estimates based on short field programs.
3. We show that MO_x rates alone cannot be used to characterize the ecosystem microbial activity, as these values are scaled to the methane concentration. We instead propose the use of an average k' value, estimated from MM kinetic analyses of all the data, as an indicator of microbial activity. Such derivation generates a more realistic parameter than values based solely on replicate samples and is similar to values obtained by work-intensive time series incubations.
4. The idea that trapping of methane in the bottom water makes it more available to microbial oxidation could not be verified. Even though the residence time of central North Sea water is about 1.5–2 years (Prandle, 1984; Ursin and Andersen, 1978) and thermal stratification prevails here for 4 months and could provide sufficient time to establish a methanotrophic community, we were not able to identify these organisms in the water column. Cultured methanotrophs have a doubling time of ~ 10 h (Bani and Liesack, 2008; Khadem et al., 2010), and after the Deep Water Horizon incident in the Gulf of Mexico, Kessler et al. (2011) estimated a doubling time of 3.5 days. Even if the doubling time of methanotrophs in the field was even longer as nutrients and substrates can be limiting, a methanotrophic community could potentially develop in the central North Sea. Nonetheless, our results indicate that in a shallow sea area, stratification over a summer season of 4 months does not enhance methane oxidation sufficiently to significantly hamper methane release to the atmosphere upon water column mixing.



Author contributions. S. Mau designed study, measured methane concentrations and methane oxidation rates, calculated the fluxes, developed the model and carried out model simulations, wrote the manuscript, T. Gentz, R. Martinez, and M. Schlüter deployed the UWMS and post-processed the data, J. H. Körber, M. Römer, H. Sahling, and P. Wintersteller collected and post-processed hydroacoustic data, M. Torres interpreted methane oxidation rate data, edited manuscript, E. Helmke implemented and interpreted molecular analyses.

Acknowledgements. We are indebted to the captain, crew, and scientific research party of the research vessel *Heincke* (cruise HE406 and HE413), especially to the organizer Sabine Kasten and Gerhard Bohrmann. We like to thank Sven Klüber, Eva Kirschenmann, and Monica Wiebe for their help collecting and analyzing samples on board and in the laboratory. We are grateful to Tessa Clemes from Alfred-Wegener-Institute for Marine and Polar Research (Bremerhaven, Germany), who implemented the microbial analyses. We like to thank Antje Boetius, Gunter Wegener, and Mirja Meiners from the Max Planck Institute for Marine Microbiology (Bremen, Germany) for providing scientific equipment and laboratory support for oxidation rate measurements. This work is part of the DFG project "Limitations of Marine Methane Oxidation" (MA 3961/2-1).

References

- Baani, M. and Liesack, W.: Two isozymes of particulate methane monooxygenase with different methane oxidation kinetics are found in *Methylocystis* sp. strain SC2, *P. Natl. Acad. Sci. USA*, 105, 10203–10208, 2008.
- Bange, H. W.: Nitrous oxide and methane in European coastal waters, *Estuar. Coast. Shelf S.*, 70, 361–374, 2006.
- Bange, H. W., Bartell, U. H., Rapsomanikis, S., and Andreae, M. O.: Methane in the Baltic and North Seas and a reassessment of the marine emissions of methane, *Global Biogeochem. Cy.*, 8, 465–480, 1994.

Seasonal methane accumulation and release from a gas emission site

S. Mau et al.

Title Page

Abstract

Introduction

Conclusions

References

Tables

Figures



Back

Close

Full Screen / Esc

Printer-friendly Version

Interactive Discussion



Seasonal methane accumulation and release from a gas emission site

S. Mau et al.

[Title Page](#)[Abstract](#)[Introduction](#)[Conclusions](#)[References](#)[Tables](#)[Figures](#)[◀](#)[▶](#)[◀](#)[▶](#)[Back](#)[Close](#)[Full Screen / Esc](#)[Printer-friendly Version](#)[Interactive Discussion](#)

Bell, R. J., Short, R. T., Van Amerom, F. H. W., and Byrne, R. H.: Calibration of an in situ membrane inlet mass spectrometer for measurements of dissolved gases and volatile organics in seawater, *Environ. Sci. Technol.*, 41, 8123–8128, 2007.

Bender, M. and Conrad, R.: Kinetics of methane oxidation inoxic soils, *Chemosphere*, 26, 687–769, 1993.

Berner, R. A.: Biogeochemical cycles of carbon and sulfur and their effect on atmospheric oxygen over Phanerozoic time, *Palaeogeogr. Palaeoclimatol.*, 73, 97–122, 1989.

Boetius, A., Ravensschlag, K., Schubert, C. J., Rickert, D., Widdel, F., Gieskes, A., Amann, R., Jørgensen, B. B., Witte, U., and Pfannkuche, O.: A marine microbial consortium apparently mediating anaerobic oxidation of methane, *Nature*, 407, 623–626, 2000.

Cicerone, R. J. and Oremland, R. S.: Biochemical aspects of atmospheric methane, *Global Biogeochem. Cy.*, 2, 299–327, 1988.

Denman, K. L. and Gargett, A. E.: Time and space scales of vertical mixing and advection of phytoplankton in the upper ocean, *Limnol. Oceanogr.*, 28, 801–815, 1983.

Eckert, W. and Conrad, R.: Sulfide and methane evolution in the hypolimnion of a subtropical lake: a three-year study, *Biogeochemistry*, 82, 67–76, 2007.

Elsaied, H. E., Hayashi, T., and Naganuma, T.: Molecular analysis of deep-sea hydrothermal vent aerobic methanotrophs by targeting genes of 16S rRNA and particulate methane monooxygenase, *Mar. Biotechnol.*, 6, 503–509, 2004.

Etiopie, G., Lassey, K. R., Klusman, R. W., and Boschi, E.: Reappraisal of the fossil methane budget and related emission from geologic sources, *Geophys. Res. Lett.*, 35, L09307, 2008.

Ford, P. W., Boon, P. I., and Lee, K.: Methane and oxygen dynamics in a shallow floodplain lake: the significance of period stratification, *Hydrobiologia*, 485, 97–110, 2002.

Gentz, T.: Distribution and fate of methane released from submarine sources – Results of measurements using an improved in situ mass spectrometer, doctoral thesis, Geosciences, University Bremen, 173 pp., 2013.

Gentz, T. and Schlüter, M.: Underwater cryotrap-membrane inlet system (CT-MIS) for improved in situ analysis of gases, *Limnol. Oceanogr.-Meth.*, 10, 317–328, 2012.

Gentz, T., Damm, E., Schneider von Deimling, J., Mau, S., McGinnis, D. F., and Schlüter, M.: A water column study of methane around gas flares located at the West Spitsbergen continental margin, *Cont. Shelf Res.*, 72, 107–118, doi:10.1016/j.csr.2013.07.013, 2013.

Gerdes, B., Brinkmeyer, R., Dieckmann, G., and Helmke, E.: Influence of crude oil on changes of bacterial communities in Arctic sea-ice, *FEMS Microbiol. Ecol.*, 53, 129–139, 2005.

Grunwald, M., Dellwig, O., Beck, M., Dippner, J. W., Freund, J. A., Kohlmeier, C., Schnetger, B., and Brumsack, H.-J.: Methane in the southern North Sea: sources, spatial distribution and budgets, *Estuar. Coast. Shelf S.*, 81, 445–456, 2009.

Gülzow, W., Rehder, G., Schneider v. Deimling, J., Seifert, T., and Tóth, Z.: One year of continuous measurements constraining methane emissions from the Baltic Sea to the atmosphere using a ship of opportunity, *Biogeosciences*, 10, 81–99, doi:10.5194/bg-10-81-2013, 2013.

Holt, J. and Umlauf, L.: Modelling the tidal mixing fronts and seasonal stratification of the Northwest European Continental shelf, *Cont. Shelf Res.*, 28, 887–903, 2008.

IPCC: Climate Change 2013 – The Physical Science Basis – Contribution of Working Group I to the Fifth Assessment Report of the Intergovernmental Panel on Climate Change, Cambridge University Press, Cambridge, 2013.

Judd, A. G., Davies, G., Wilson, J., Holmes, R., Baron, G., and Bryden, I.: Contributions to atmospheric methane by natural seepages on the U. K. continental shelf, *Mar. Geol.*, 140, 427–455, 1997.

Kankaala, P., Taipale, S., Nykänen, H., and Jones, R. I.: Oxidation, efflux, and isotopic fractionation of methane during autumnal turnover in a polyhumic, boreal lake, *J. Geophys. Res.*, 112, G02003, 2007.

Kessler, J. D., Valentine, D. L., Redmond, M. C., Du, M., Chan, E. C., Mendes, S. D., Quiroz, E. W., Villanueva, C. J., Shusta, S. S., Werra, L. M., Yvon-Lewis, S. A., and Weber, T. C.: A persistent oxygen anomaly reveals the fate of spilled methane in the deep Gulf of Mexico, *Science*, 331, 312–315, 2011.

Khadem, A. F., Pol, A., Jetten, M. S. M., and Op den Camp, H. J. M.: Nitrogen fixation by the verrucomicrobial methanotroph “*Methylacidiphilum fumariolicum*” SolV, *Microbiology*, 156, 1052–1059, 2010.

Killops, S. D. and Killops, V. J.: *An Introduction to Organic Geochemistry*, Longman, Essex, UK, 1993.

King, G. M.: Ecological aspects of methane oxidation, a key determinant of global methane dynamics, *Adv. Microb. Ecol.*, 12, 432–468, 1992.

Koschel, R.: Untersuchungen zur Phosphataffinität des Planktons in der euphotischen Zone von Seen, *Limnologica*, 12, 141–145, 1980.

Largier, J. L.: Considerations in estimating larval dispersal distances from oceanographic data, *Ecol. Appl.*, 13, 71–89, 2003.

BGD

11, 18003–18044, 2014

Seasonal methane accumulation and release from a gas emission site

S. Mau et al.

Title Page

Abstract

Introduction

Conclusions

References

Tables

Figures



Back

Close

Full Screen / Esc

Printer-friendly Version

Interactive Discussion



Seasonal methane accumulation and release from a gas emission site

S. Mau et al.

Title Page

Abstract

Introduction

Conclusions

References

Tables

Figures



Back

Close

Full Screen / Esc

Printer-friendly Version

Interactive Discussion



Mau, S., Valentine, D. L., Clark, J. F., Reed, J., Camilli, R., and Washburn, L.: Dissolved methane distributions and air–sea flux in the plume of a massive seep field, Coal Oil Point, California, *Geophys. Res. Lett.*, 34, L22603, 2007.

Mau, S., Heintz, M. B., and Valentine, D. L.: Quantification of CH₄ loss and transport in dissolved plumes of the Santa Barbara Channel, California, *Cont. Shelf Res.*, 32, 110–120, 2012.

Mau, S., Blees, J., Helmke, E., Niemann, H., and Damm, E.: Vertical distribution of methane oxidation and methanotrophic response to elevated methane concentrations in stratified waters of the Arctic fjord Storfjorden (Svalbard, Norway), *Biogeosciences*, 10, 6267–6278, doi:10.5194/bg-10-6267-2013, 2013.

McDonald, I. R. and Murrell, J. C.: The particulate methane monooxygenase gene *pmoA* and its use as a functional gene probe for methanotrophs, *FEMS Microbiol. Lett.*, 156, 205–210, 1997.

McDonald, I. R., Bodrossy, L., Chen, Y., and Murrell, J. C.: Molecular ecology techniques for the study of aerobic methanotrophs, *Appl. Environ. Microb.*, 74, 1305–1315, 2008.

McGillis, W., R., Edson, J., B., Ware, J., D., Dacey, J., W. H., Hare, J., E., Fairall, C., W., and Wanninkhof, R.: Carbon dioxide flux techniques performed during GasEx-98, *Mar. Chem.*, 75, 267–280, 2001.

McGinnis, D. F., Greinert, J., Artemov, Y., Beaubien, S. E., and Wuest, A.: Fate of rising methane bubbles in stratified waters: how much methane reaches the atmosphere?, *J. Geophys. Res.*, 111, 15, 2006.

Muyzer, G., de Waal, E., and Uitterlinden, A.: Profiling of complex microbial populations by denaturing gradient gel electrophoresis analysis of polymerase chain reaction-amplified genes coding for 16S rRNA, *Appl. Environ. Microb.*, 59, 695–700, 1993.

Niemann, H., Elvert, M., Hovland, M., Orcutt, B., Judd, A., Suck, I., Gutt, J., Joye, S., Damm, E., Finster, K., and Boetius, A.: Methane emission and consumption at a North Sea gas seep (Tommeliten area), *Biogeosciences*, 2, 335–351, doi:10.5194/bg-2-335-2005, 2005.

Pack, M. A., Heintz, M. B., Reeburgh, W. S., Trumbore, S. E., Valentine, D. L., Xu, X., and Druffel, E. R. M.: A method for measuring methane oxidation rates using low-levels of ¹⁴C-labeled methane and accelerator mass spectrometry, *Limnol. Oceanogr.-Meth.*, 9, 245–260, 2011.

Pingree, R. D. and Griffiths, D. K.: Tidal fronts on the shelf seas around the British Isles, *J. Geophys. Res.*, 83, 4615–4622, 1978.

Seasonal methane accumulation and release from a gas emission site

S. Mau et al.

Title Page

Abstract

Introduction

Conclusions

References

Tables

Figures

◀

▶

◀

▶

Back

Close

Full Screen / Esc

Printer-friendly Version

Interactive Discussion



- Prandle, D.: A modelling study of the mixing of ^{137}Cs in the seas of the European continental shelf, *Philos. T. Roy. Soc. A*, 310, 407–436, 1984.
- Pruesse, E., Peplies, J., and Glöckner, F. O.: SINA: accurate high-throughput multiple sequence alignment of ribosomal RNA genes, *Bioinformatics*, 28, 1823–1829, 2012.
- 5 Reeburgh, W. S., Ward, B. B., Whalen, S. C., Sandbeck, K. A., Kilpatrick, K. A., and Kerkhof, L. J.: Black Sea methane geochemistry, *Deep-Sea Res.*, 38, 1189–1210, 1991.
- Rehder, G., Keir, R. S., Suess, E., and Pohlmann, T.: The multiple sources and patterns of methane in North Sea waters, *Aquat. Geochem.*, 4, 403–427, 1998.
- Schlüter, M. and Gentz, T.: Application of membrane inlet mas spectrometry for online and in situ analysis of methane in aquatic environments, *J. Am. Soc. Mass Spectr.*, 19, 1395–1402, 10 2008.
- Schneider von Deimling, J., Rehder, G., Greinert, J., McGinnis, D. F., Boetius, A., and Linke, P.: Quantification of seep-related methane gas emissions at Tommeliten, North Sea, *Cont. Shelf Res.*, 31, 876–878, 2011.
- 15 Schroot, B. M., Klaver, G. T., and Schuettenhelm, T. E.: Surface and subsurface expressions of gas seepage to the seabed – examples from the southern North Sea, *Mar. Petrol. Geol.*, 22, 499–515, 2005.
- Scranton, M. I. and McShane, K.: Methane fluxes in the southern North Sea: the role of European rivers, *Cont. Shelf Res.*, 11, 37–52, 1991.
- 20 Short, R. T., Fries, D. P., Kerr, M. L., Lembke, C. E., Toler, S. K., Wenner, P. G., and Byrne, R. H.: Underwater mass spectrometers for in situ chemical analysis of the hydrosphere, *J. Am. Soc. Mass Spectr.*, 12, 676–682, 2001.
- Sundermeyer, M. A. and Price, J. F.: Lateral mixing and the North Atlantic tracer release experiment: observations and numerical simulations of Lagrangian particles and a passive tracer, *J. Geophys. Res.*, 103, 21481–21497, 1998.
- 25 Tavormina, P. L., Ussler III, W., and Orphan, V. J.: Planktonic and sediment-associated aerobic methanotrophs in two seep systems along the North American Margin, *Appl. Environ. Microb.*, 74, 3985–3995, 2008.
- Ursin, E. and Andersen, K. P.: A model of the biological effects of eutrophication in the North Sea, *Rap. Proces.*, 172, 366–377, 1978.
- 30 Valentine, D. L.: Emerging topics in marine methane biogeochemistry, *Ann. Rev. Mar. Sci.*, 3, 147–171, 2011.

Seasonal methane accumulation and release from a gas emission site

S. Mau et al.

[Title Page](#)[Abstract](#)[Introduction](#)[Conclusions](#)[References](#)[Tables](#)[Figures](#)[Back](#)[Close](#)[Full Screen / Esc](#)[Printer-friendly Version](#)[Interactive Discussion](#)

Valentine, D. L., Blanton, D. C., Reeburgh, W. S., and Kastner, M.: Water column methane oxidation adjacent to an area of active hydrate dissociation, Eel River Basin, *Geochim. Cosmochim. Ac.*, 65, 2633–2640, 2001.

Valentine, D. L., Kessler, J. D., Redmond, M. C., Mendes, S. D., Heintz, M. B., Farwell, C., Hu, L., Kinnaman, F. S., Yvon-Lewis, S., Du, M., Chan, E. W., Tigreros, F. G., and Villanueva, C. J.: Propane respiration jump-starts microbial response to a deep oil spill, *Science*, 330, 208–211, 2010.

Wasmund, K., Kurtboke, D. I., Burns, K. A., and Bourne, D. G.: Microbial diversity in sediments associated with a shallow methane seep in the tropical Timor Sea of Australia reveals a novel aerobic methanotroph diversity, *FEMS Microbiol. Ecol.*, 68, 142–151, 2009.

Wenner, P. G., Bell, P. G., van Amerom, F. H. W., Toler, S. K., Edkins, J. E., Hall, M. L., Koehn, K., Short, R. T., and Byrne, R. H.: Environmental chemical mapping using an underwater mass spectrometer, *Trac-Trend Anal. Chem.*, 23, 288–295, 2004.

Wiesenburg, D. A. and Guinasso, J. N. L.: Equilibrium solubilities of methane, carbon monoxide, and hydrogen in water and sea water, *J. Chem. Eng. Data*, 24, 356–360, 1979.

Wunsch, C. and Ferrari, R.: Vertical mixing, energy, and the general circulation of the oceans, *Annu. Rev. Fluid Mech.*, 36, 281–314, 2004.

Seasonal methane accumulation and release from a gas emission site

S. Mau et al.

Title Page

Abstract

Introduction

Conclusions

References

Tables

Figures

◀

▶

◀

▶

Back

Close

Full Screen / Esc

Printer-friendly Version

Interactive Discussion



Table 1. Classification of partial 16S rRNA gene sequences (Fig. 6) to bacterial taxa performed with the Silva classifier (Pruesse et al., 2012). The confidence value (0–1) for assignment at the level of class and genus is given in parentheses.

No.	Class	Family
1	Alphaproteobacteria (0.4)	SAR11 clade (0.2)
2	Cyanobacteria (1)	<i>Chloroplast</i> (1)
3	Alphaproteobacteria (1)	<i>Rhodobacteraceae</i> (1)
4	Bacteroidetes incertae sedis (0.43)	<i>Marinifilum</i> (0.4)
5	Alphaproteobacteria (1)	<i>Rhodobacteraceae</i> (1)
6	Alphaproteobacteria (1)	<i>Rhodobacteraceae</i> (1)
7	Alphaproteobacteria (1)	<i>Rhodobacteraceae</i> (1)
8	Cyanobacteria (1)	<i>Synechococcus</i> (1)
9	Cyanobacteria (1)	<i>Synechococcus</i> (1)
10	Gammaproteobacteria (1)	<i>Pseudoalteromonadaceae</i> (1)
11	Proteobacteria (0.36)	
12	Alphaproteobacteria (1)	<i>Rhodospirillaceae</i> (0.8)
13	Alphaproteobacteria (0.91)	<i>Rhodospirillaceae</i> (0.7)

Seasonal methane accumulation and release from a gas emission site

S. Mau et al.

Table 2. Comparison of highest methane concentrations, methane oxidation rates, and sea–air fluxes from different locations.

Location	Methane concentration up to nM	MO _x -rate nM day ⁻¹	SAF nmol m ⁻² s ⁻¹	Reference
Seep sites				
Central North Sea	1628	0.04–840	0.02–8.3	this study
Coal Oil Point, Santa Barbara Basin	1900	0.02–30	1.8	Mau et al. (2012); Pack et al. (2011)
Tommeliten, North Sea	268		10.8*	Schneider von Deimling et al. (2011)
West of Prins Karls Forland, Svalbard	524	up to 0.8		Gentz et al. (2013)
Gulf of Mexico	180 000	up to 820		Valentine et al. (2010)
Eel River Basin	300	0.002–0.8		Valentine et al. (2001)
Overall areas				
Baltic Sea	38		0.008–0.2	Gülzow et al. (2013)
Southern Bight of the North Sea	372	0.0002–0.3	0.07–7	Scranton and McShane (1991)
General European shelf estimate	21		0.11–0.24	Bange (2006)
Lakes				
Floodplain lake in south-eastern Australia	50 000		8.3–2700	Ford et al. (2002)
Polyhumic lake in southern Finland	150 000	30–14 400	0.5–695	Kankaala et al. (2007)
The subtropical Lake Kinneret in Israel	450 000			Eckert and Conrad (2007)

* Direct transport via bubbles

Title Page

Abstract

Introduction

Conclusions

References

Tables

Figures

⏪

⏩

◀

▶

Back

Close

Full Screen / Esc

Printer-friendly Version

Interactive Discussion



Seasonal methane accumulation and release from a gas emission site

S. Mau et al.

Title Page

Abstract

Introduction

Conclusions

References

Tables

Figures



Back

Close

Full Screen / Esc

Printer-friendly Version

Interactive Discussion

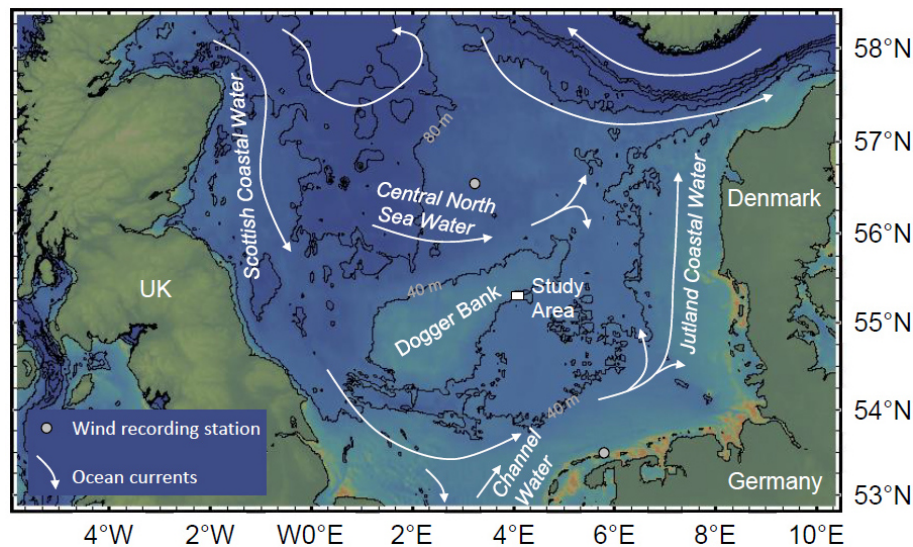


Figure 1. Location of the study area in the central North Sea. The main currents are shown following Howarth (2001). The map was drawn using GeoMapApp with 40 m contours.

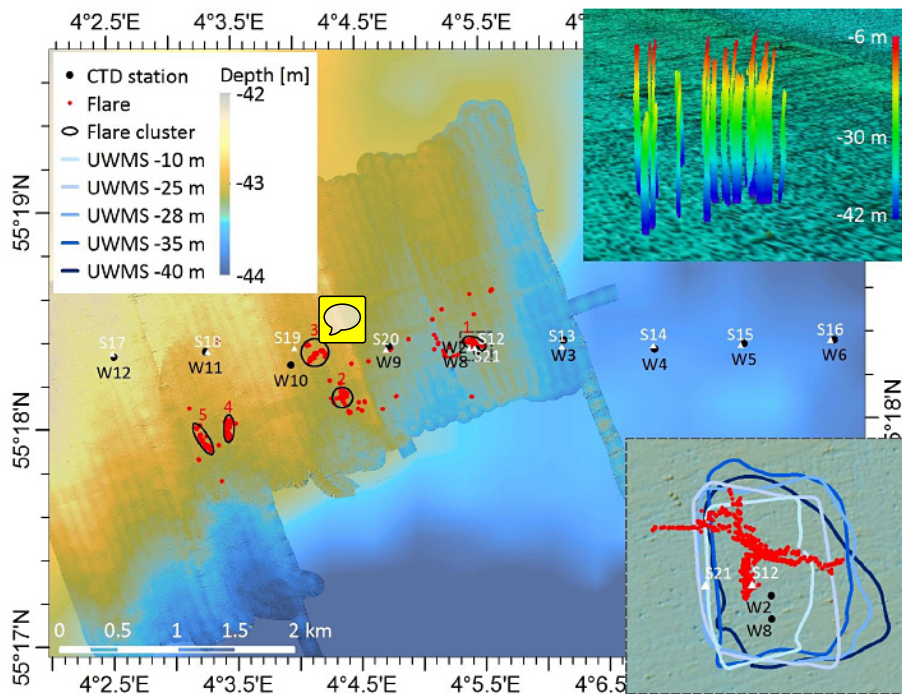


Figure 2. Overview of gas flares mapped in January 2014 and CTD stations sampled in July 2013 and January 2014. Flares cluster in 5 distinct areas (cluster 1–5) and reach to 6 m from the sea surface (e.g. cluster 2 in upper right insert), which corresponds to the echosounder’s transducer depth. Hence, most likely the gas transport extends to the sea surface. Cluster 1 corresponds to the gas seep area investigated by Gentz (2013) (lower right insert).

Seasonal methane accumulation and release from a gas emission site

S. Mau et al.

Title Page	
Abstract	Introduction
Conclusions	References
Tables	Figures
◀	▶
◀	▶
Back	Close
Full Screen / Esc	
Printer-friendly Version	
Interactive Discussion	



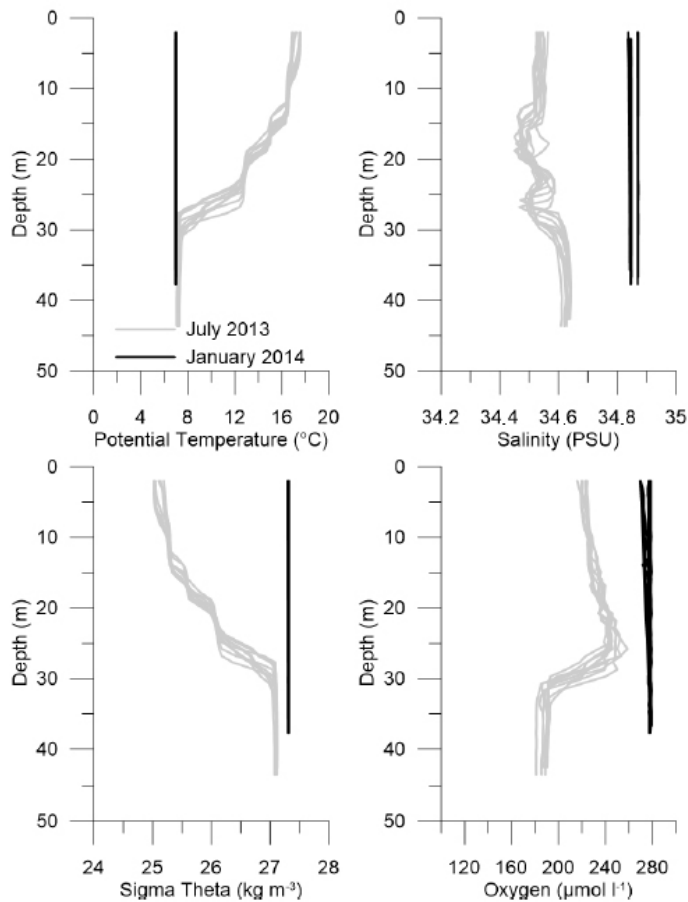


Figure 3. Depth profiles of potential temperature, salinity, density (sigma theta), and oxygen for all stations in both summer and winter field programs.

Seasonal methane accumulation and release from a gas emission site

S. Mau et al.

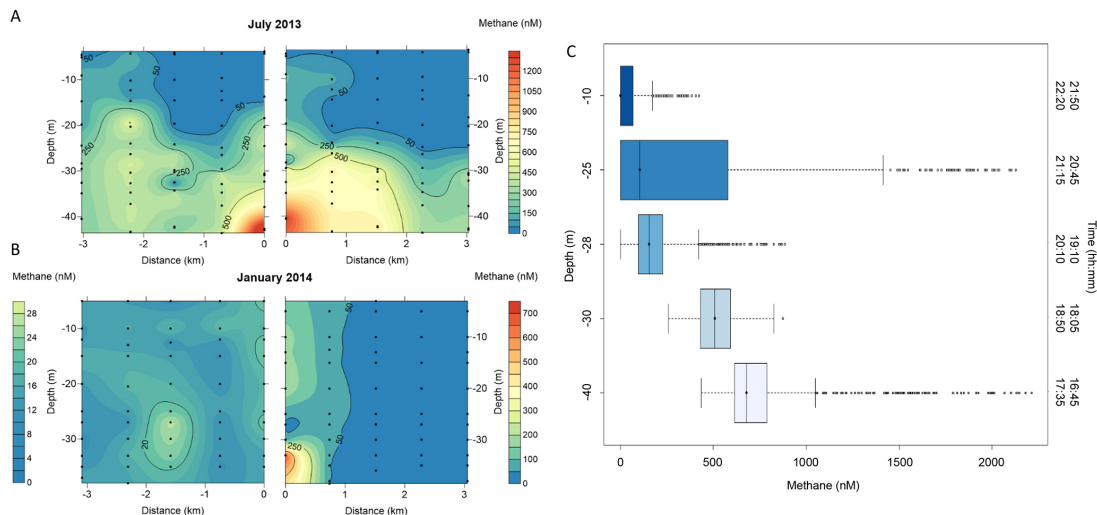


Figure 4. (a), (b) Contour plots of the dissolved methane concentrations measured in the water column in July 2013 and January 2014. The 6 km transect was divided into an eastern (positive numbers) and western part (negative numbers) starting from the center station at 0 km. Note the different methane concentration scales, which are necessary to properly display the different concentration ranges. The black dots indicate the sampled water depths. (c) Box plot of methane concentrations recorded by UWMS on 21 July 2013. The times on the right side refer to the start and end times of the rectangular transects the UWMS was towed along in the vicinity of flare cluster 1 (Fig. 2) at each water depth. Profiles obtained with UWMS are consistent with discrete water sampling data.

Seasonal methane accumulation and release from a gas emission site

S. Mau et al.

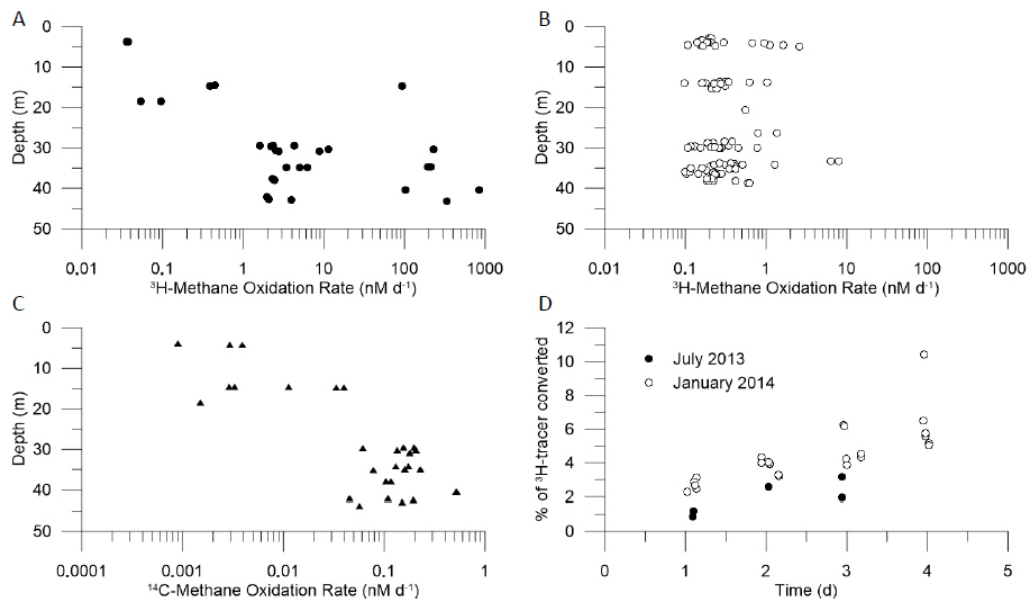


Figure 5. (a)–(c) Methane oxidation rates vs. water depth measured with ³H-methane in July 2013 (a), with ³H-methane in January 2014 (b), and using ¹⁴C-methane as tracer in July 2013 (c). (d) Time series of water samples collected during both field programs and incubated with ³H-methane.

[Title Page](#)
[Abstract](#)
[Introduction](#)
[Conclusions](#)
[References](#)
[Tables](#)
[Figures](#)
[Back](#)
[Close](#)
[Full Screen / Esc](#)
[Printer-friendly Version](#)
[Interactive Discussion](#)

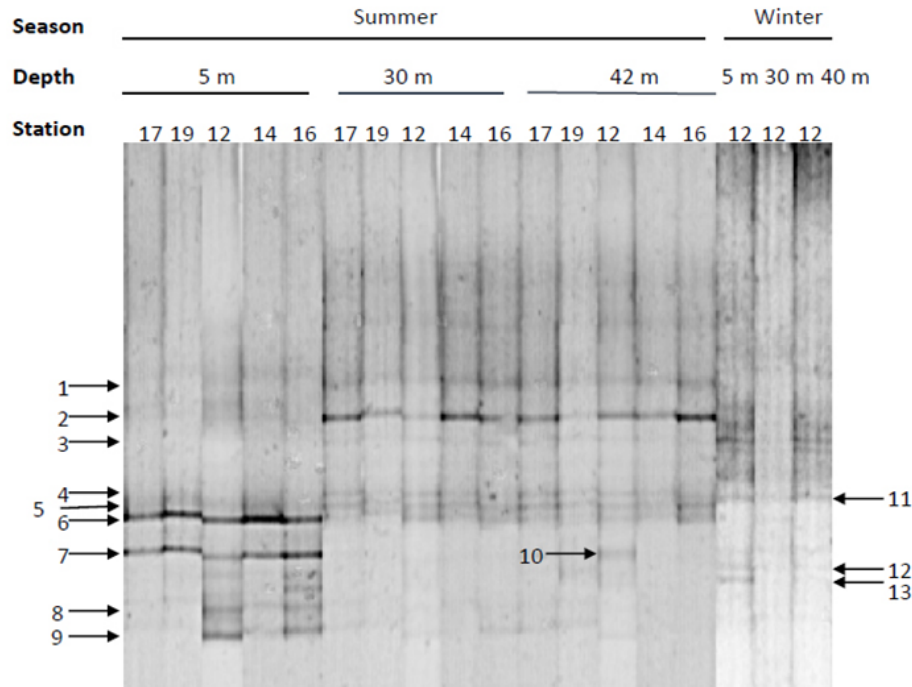


Figure 6. DGGE profile of 16S rRNA gene fragments of samples from different depth and stations in the central North Sea. Numbers on the lines indicate excised and successfully sequenced DGGE bands, whose phylogenetic assignment is listed in Table 1.

Seasonal methane accumulation and release from a gas emission site

S. Mau et al.

[Title Page](#)

[Abstract](#) [Introduction](#)

[Conclusions](#) [References](#)

[Tables](#) [Figures](#)

[◀](#) [▶](#)

[◀](#) [▶](#)

[Back](#) [Close](#)

[Full Screen / Esc](#)

[Printer-friendly Version](#)

[Interactive Discussion](#)



Seasonal methane accumulation and release from a gas emission site

S. Mau et al.

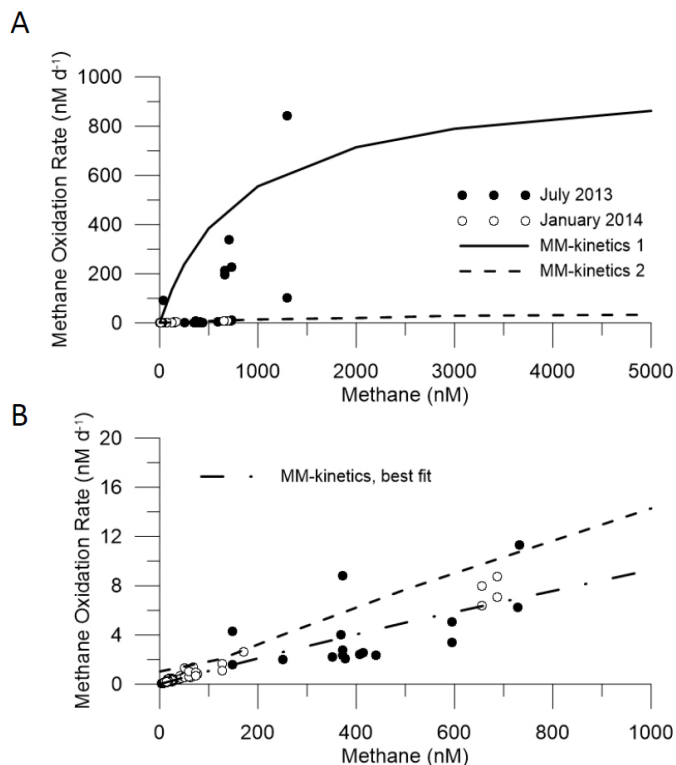


Figure 7. Methane oxidation rate vs. methane concentration. **(a)** Michaelis-Menten kinetics of Eq. (6) (MM-kinetics) using the parameters $v_{\max} = 1000 \text{ nM day}^{-1}$ and $K_m = 800 \text{ nM}$ for curve MM-kinetics 1 and $v_{\max} = 100 \text{ nM day}^{-1}$ and $K_m = 12000 \text{ nM}$ for curve MM-kinetics 2. Together, both curves encompass the range of the enzyme kinetics available. **(b)** Close up of the data for MO_x -rates $< 20 \text{ nM day}^{-1}$ and MM-kinetics 2 in that range. The best fitting MM-kinetics yield values of $v_{\max} = 65 \text{ nM day}^{-1}$ and $K_m = 6000 \text{ nM}$.

Title Page

Abstract

Introduction

Conclusions

References

Tables

Figures

◀

▶

◀

▶

Back

Close

Full Screen / Esc

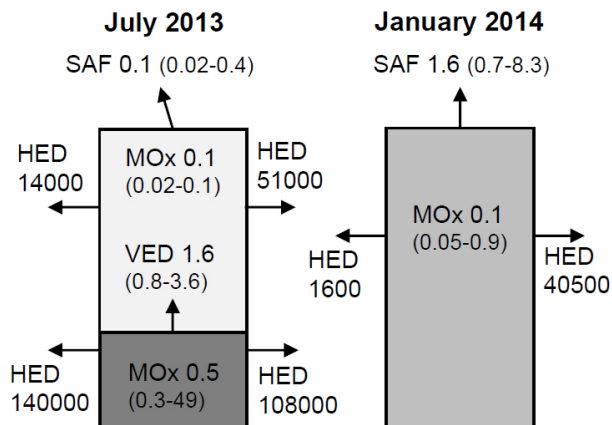
Printer-friendly Version

Interactive Discussion



Seasonal methane accumulation and release from a gas emission site

S. Mau et al.



SAF – Sea Air Flux
 MOx – Methane Oxidation rate
 VED – Vertical Eddy Diffusion
 HED – Horizontal Eddy Diffusion
 Median of estimates (range of estimates)

Figure 8. Sketch of transport and loss terms estimated for the study area in $\text{nmol m}^{-2} \text{s}^{-1}$.

Title Page

Abstract

Introduction

Conclusions

References

Tables

Figures

◀

▶

◀

▶

Back

Close

Full Screen / Esc

Printer-friendly Version

Interactive Discussion



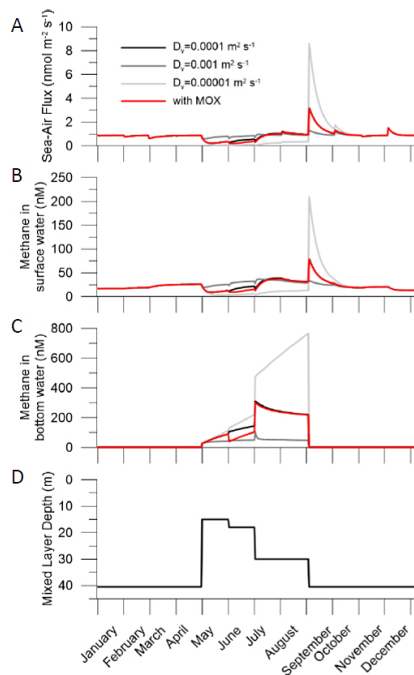


Figure 9. Model results over the course of a year. The mixed layer depth (**d**) shows the time period of water column stratification from May until August. The mixed layer deepens during this time until the entire water column is mixed again. During stratification, the water column is separated in surface (**b**) and bottom water (**c**) whereas during the rest of the year the entire water column is well mixed with methane concentrations shown in (**b**). Panel (**a**) displays the sea-air flux based on monthly mean wind speed derived from the stations shown in Fig. 1. Model simulations including solely vertical transport processes are shown as gray lines, which illustrate the range due to different D_v values (see text). The model simulation based on methane oxidation in addition to vertical transport is shown as a red line.

Seasonal methane accumulation and release from a gas emission site

S. Mau et al.

Title Page

Abstract Introduction

Conclusions References

Tables Figures

◀ ▶

◀ ▶

Back Close

Full Screen / Esc

Printer-friendly Version

Interactive Discussion

